Spectral shifts in tip-induced light from plasmonic nanoparticles in air

Mario Zapata-Herrera, Benoît Rogez, Sylvie Marguet, Gérald Dujardin, Elizabeth Boer-Duchemin, Eric Le Moal

Spectral shifts in tip-induced light from plasmonic nanoparticles in air

Mario Zapata-Herrera,[1] Benoît Rogez,[2,*] Sylvie Marguet,[3] Gérald Dujardin,[2] Elizabeth Boer-Duchemin,[2] and Eric Le Moal[2,†]

[1]*Donostia International Physics Center (DIPC), Donostia-San Sebastián 20018, Spain*
[2]*Université Paris-Saclay, CNRS, Institut des Sciences Moléculaires d'Orsay, 91405 Orsay, France*
[3]*Université Paris-Saclay, CEA, CNRS, NIMBE, 91191 Gif-sur-Yvette, France*

(Received 1 February 2024; revised 5 April 2024; accepted 8 April 2024; published 26 April 2024)

In this article, we carry out an in-depth study of the scanning tunneling microscopy-induced luminescence spectra (STML) of individual plasmonic nanoparticles measured in air. When compared to the results of far-field light scattering measured under the same ambient conditions, the STML measurements show spectral shifts and peak broadening of hundreds of meV, even when a nonplasmonic tip is used for STML. We simulate the near-field excitation and the effect of the tip using the finite-element method and show that these effects alone cannot explain the spectral shifts and peak broadening observed for STML experiments in air. However, the experimental results are well reproduced in the numerical simulations if the screening effect of a water meniscus bridge present in the tip-nanoparticle gap is considered. Our results pave the way for finer interpretations of STML experiments in air, where ignoring this additional screening effect can lead to an incorrect mode assignment of the observed resonances.

DOI: 10.1103/PhysRevB.109.155433

I. INTRODUCTION

Probing the optical properties of plasmonic nanoparticles (NPs) on the nanometer scale has become crucial in nanophotonics, e.g., to engineer their near-field coupling to other plasmonic NPs or to quantum emitters. Various techniques have been developed to carry out such nanoscale investigations, either using photons [1–4] or electrons [5–16] to excite the plasmon modes of metal NPs. Among such techniques, inelastic electron tunneling in a scanning tunneling microscope (STM) is a local, low-energy, electrical excitation source for exciting plasmonic nanostructures. Such a source is broadband in frequency in the visible and infrared ranges [16–25]. STM-induced luminescence spectroscopy (STML) and pixel-by-pixel mapping have been used under ultrahigh vacuum conditions to investigate the spectral and spatial distribution of the plasmon modes of metal NPs [7,14,26–30]. The STM tip has been reported to affect the plasmon resonances of the NPs under such conditions [31]. Such tip effects have also been discussed in the context of scattering-type scanning near-field optical microscopy [32].

Moreover, since the STM may be used in air, it can be combined with optical microscopy in order to spatially and angularly resolve the STM-induced luminescence [33–37]. When working in air, not only tip-sample coupling but also the adsorption of water and the formation of a water meniscus bridge in the tip-sample gap [38–41] are expected to modify the optical response of the NP [42]. The presence of such a water bridge in the tip-sample gap has been theoretically explained [43–46] and its resulting effects have also been experimentally observed in previous atomic force microscopy [47–53] and scanning near-field optical microscopy-based studies [54–56]. Discrepancies (e.g., spectral shifts) between the optical response of metal NPs measured by STML in air and their optical response measured using far-field light scattering spectroscopy have been reported [13,57]. However, the microscopic mechanism behind these discrepancies and the relative contribution of this effect with respect to other factors present both in air and vacuum, i.e., tip-sample coupling and multipolar contributions, have so far not been studied.

The effect of a water bridge on the properties of tunnel nanojunctions has been previously studied for plasmonic nanojunctions, i.e., junctions formed by a nanometer gap between two plasmonic NPs [42] or between a plasmonic tip and a plasmonic surface in an STM [39]. The optical response of such junctions is dominated by the resonances of the so-called nanocavity (or tip-induced) gap plasmons [18,19], which are highly sensitive to the gap geometry and dielectric properties [4,58,59]. Gap plasmon resonances are redshifted in the presence of water in the gap, as compared to vacuum, due to dielectric screening [42]. Additionally, bridging the gap with water decreases the electric resistivity of the tunnel junction. In the constant current mode of an STM, this effect is compensated by an increase of the tip-sample distance, which blueshifts the gap plasmon resonances [39]. These previous studies cannot be used to explain the effects observed in STML experiments where a nonplasmonic tip is used, as in the present study, due to the absence of gap plasmons in the tunnel junction. Indeed, when a nonplasmonic tip is used to excite the modes of a plasmonic NP, the spectrum of the resulting light

*Present address: Laboratory Light, nanomaterials and nanotechnologies - L2n, University of Technology of Troyes - CNRS EMR 7004, 12 rue Marie Curie, 10000 Troyes, France.
†eric.le-moal@universite-paris-saclay.fr

is dominated by the resonances of the NP plasmons [13]. In previous STML studies on gold NPs in air [13,57], the water bridge effect was not taken into account in the interpretation of the measured STML spectra.

In this work, we experimentally and numerically analyze the discrepancies between the STML spectra of individual plasmonic NPs and the resonances of their plasmon modes as measured using far-field light scattering spectroscopy. The NPs are monocrystalline gold nanocubes dispersed on a transparent conductive substrate. All experiments are carried out in air under the same ambient conditions. We find that the emission peaks in the STML spectra are redshifted by hundreds of meV relative to the plasmon resonances of the NPs inferred from light scattering measurements. In the absence of a model for this effect, these shifts lead to an erroneous assignment of the STML peaks to the in-plane and out-of-plane dipolar plasmon modes of the NPs. Based on numerical simulations using the finite-element method (FEM) implemented in COMSOL MULTIPHYSICS, we highlight the effects of the tip and of the near-field excitation, which are present for experiments in both air and vacuum. Moreover, we show that reproducing the energy shifts and peak broadening observed for STML in air requires the inclusion of a water bridge between the tip and the sample. Using this more realistic model leads to the correct assignment of the STML peaks to particular plasmon modes of the NP.

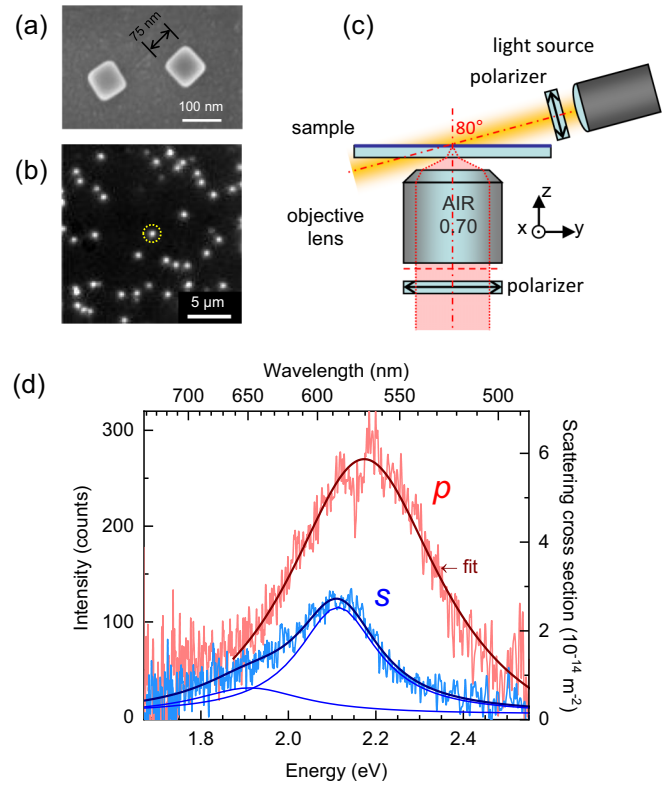

FIG. 1. (a) Scanning electron micrograph of two nanocubes, 75 nm in edge length, showing their regular shape and rounded corners. (b) Dark-field optical microscopy image of individual nanocubes, in gray scale. (c) Experimental setup used for dark-field optical spectroscopy of single NPs upon illumination with linearly polarized white light at grazing incidence. Light is collected through the substrate. (d) Light scattering spectra of the single NP selected in image (b), measured using the setup described in (c). *s* and *p* refer to the orientation of the polarization of the excitation field, either perpendicular (*s*) or parallel (*p*) to the plane of incidence (*yz*) defined in (c). Thus the spectra labeled *s* and *p* correspond to the in-plane (along *x*) and out-of-plane (along *z*) dipolar resonances of the NP, respectively. The experimental data are background subtracted, corrected for both the power spectrum of the source and for the detection efficiency of the setup and are fit with Lorentzian profiles.

II. METHODS

A. Experiments

Figure 1(a) is a scanning electron micrograph (SEM) of two NPs from the sample used in this study. The NPs are chemically synthesized using the method that is described in Ref. [60]. The resulting NPs are monocrystalline gold nanocubes, whose edge length is 75 nm on average and whose edges and corners are rounded with typical radii of curvature of 10 nm (see also Ref. [61]). The NPs are dispersed on a transparent conductive substrate, i.e., a glass coverslip coated with an 85-nm-thick indium-tin oxide (ITO) layer (see Fig. S1 in the Supplemental Material [62]). STML, optical microscopy, and SEM measurements are carried out using the same sample.

Far-field light scattering spectra of individual NPs are measured using dark-field optical microscopy (DFM) under grazing incident illumination (i.e., at 80° from the normal to the surface) using a collimated white light beam. The experimental setup [13,35,57] is schematized in Fig. 1(c). The light scattered by the NPs is collected in transmission using an air microscope objective of numerical aperture NA = 0.7. The spectrum of the light scattered by individual NPs is measured using two different polarizations of the incident light, i.e., with the electric field perpendicular (*s*) or parallel (*p*) to the plane of incidence, in order to probe the in-plane (along *x*) and out-of-plane (along *z*) dipolar resonances of the NPs, respectively. The background is subtracted from the scattering spectra, which are subsequently divided by the power spectrum of the light source and corrected for the polarizer transmission.

Figure 2(a) shows a schematic of the experimental STML setup [33,63,64]. An air-operated STM head is mounted on top of an inverted optical microscope equipped with an oil-immersion objective of high numerical aperture (NA = 1.45) and the STM-induced light is collected through the glass substrate. All the experimental STM and STML data shown below are obtained using the same STM tip, which is an electrochemically etched tungsten wire. All STML data are measured at a sample bias of 2.75 V and current set point of 100 pA. We assume that the power spectrum of the STML excitation source varies proportionally to $(e|V| - h\nu)$, where e, $|V|$, and $h\nu$ are the elementary charge of the electron, the bias voltage applied to the STM junction, and the photon energy, respectively [19]. For comparison with DFM spectra and scattering cross section calculations, all the STML data are corrected for the frequency dependence of the STM excitation source mentioned above. Thus the experimental spectra are divided by a factor $(h\nu - 2.75\ \text{eV})$ and a flat power distribution is considered in the numerical simulations of STML

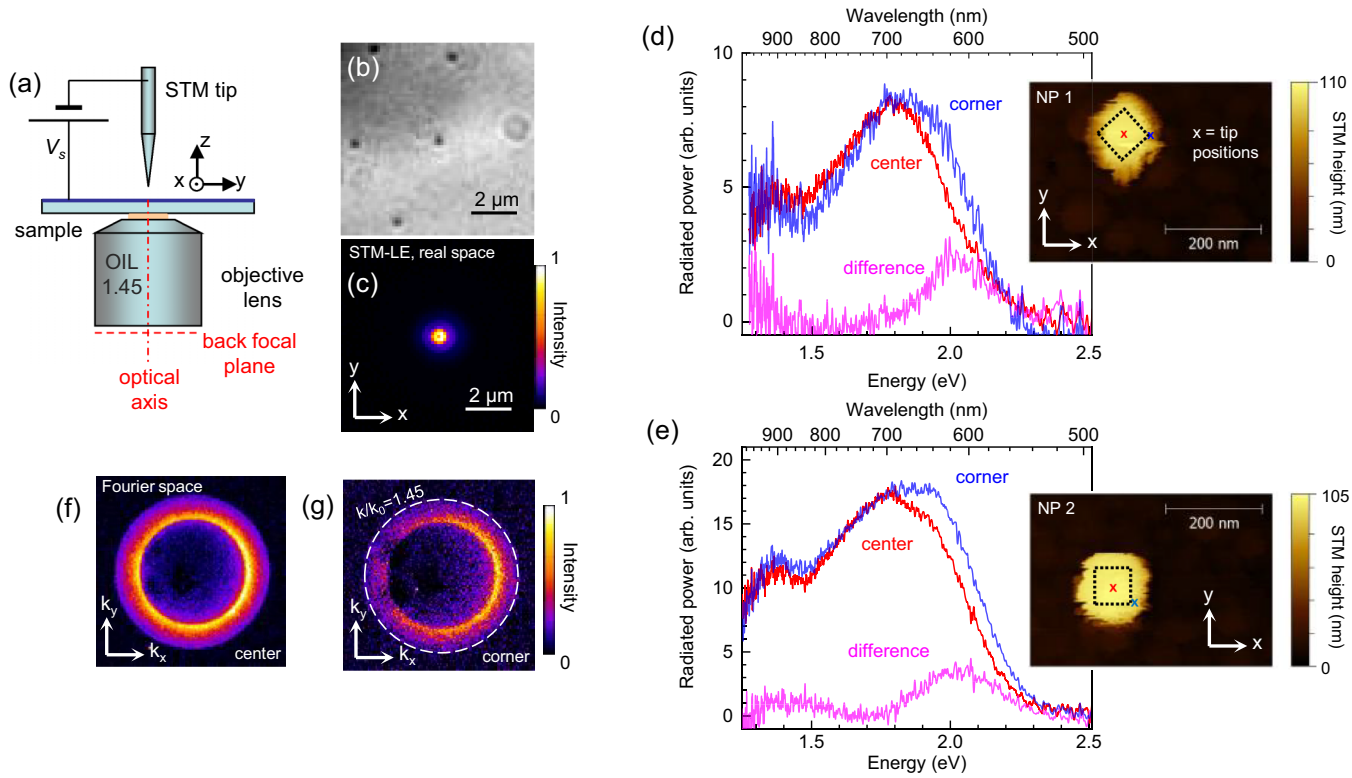

FIG. 2. (a) Experimental setup used for optical microscopy of the STML of NPs on a transparent conductive substrate. (b) Bright-field optical microscopy image of individual nanocubes, in gray scale. (c) Real-space optical microscopy image of the STM-induced luminescence (STML) of the same area upon electrical excitation of the single nanocube in the center of the image shown in (b) (false-color scale). STML spectra of (d) the nanocube shown in image (c) ("NP 1"); (e) STML spectra of another nanocube of the same sample ("NP 2"). Sample bias in both cases is 2.75 V, current set point is 100 pA, and acquisition time is 300 s. The STM tip is located in the center and on the corner of the cube's top face, as indicated on the STM topography image in the inset. The experimental data are corrected for both the theoretical power spectrum of the inelastic tunneling current and for the detection efficiency of the setup. The STML spectra measured at the "center" and "corner" tip positions are expressed in arbitrary units, i.e., they are not normalized with respect to the tunneling current. We have normalized these spectra with respect to their intensity at a photon energy of 1.81 eV, in order to highlight the difference between the two spectra. (f),(g) Fourier-space optical microscopy images of the STML of the same nanocube as in (c) and (d), for "center" and "corner" tip positions (2.75 V, 100 pA, and 120 s). All the STML data shown in this figure have been obtained using the same tungsten tip.

spectra. In addition, the experimental STML spectra, initially expressed in counts per energy unit, are corrected for the detection efficiency of the setup and multiplied by the photon energy, in order to compare them with the calculated radiated power.

B. Numerical simulations

In the calculations, the excitation source (i.e., inelastic electron tunneling [17,21,65,66]) is equated to an oscillating electric dipole located at the center of the tip-sample gap and oriented along the z axis (this excitation source has a flat power spectrum). The actual STM tip is simplified as a cylindrical rod that has a spherical end of radius 30 nm. This radius of curvature was determined from electron micrographs of tungsten tips prepared using the same protocol as for the tungsten tips used to measure the STML spectra (see Fig. S2 in Ref. [57]). A realistic shape for the NP is taken into account, using the geometrical parameters inferred from Fig. 1(a), i.e., a cube that is 75 nm in edge length and has rounded edges and corners with radii of curvature of 10 nm. Charge and electric field distributions, in addition to far-field radiation fluxes, are calculated using the RF module of the COMSOL MULTIPHYSICS software suite.

III. RESULTS AND DISCUSSION

A. Experimental measurements

First, we measure the optical response of the NP using DFM (see Methods). Figure 1(b) shows a DFM image (linear gray scale), where each bright spot corresponds to a single NP. Figure 1(d) shows the light scattering spectra measured on the NP circled in Fig. 1(b). In these spectra, the resonances of the in-plane (along x) and out-of-plane (along z) dipolar plasmon modes of the NP may be seen. Because the substrate breaks the symmetry of the NP environment, the dipolar resonances of the NP along x and z are not degenerate in energy (unlike in solution). From Fig. 1(d), we determine that the in-plane and out-of-plane dipolar resonances of the NP lie at photon energies of 2.11 eV and 2.17 eV and exhibit full widths at half maximum (FWHM) of 0.29 eV and 0.37 eV, respectively. From extinction spectra measured in solution (see Fig. S2 in the Supplemental Material [62]), a resonance at 2.17 eV with a

FWHM of 0.26 eV may be estimated for the dipolar resonance of the NP.

In the following, we consider STML measurements on individual NPs of the same sample and under the same environmental conditions (i.e., in laboratory air) as the DFM measurements discussed above (see Methods). Figure 2(b) shows a brightfield (white light transmission) optical microscopy image of the sample, where each dark spot is a single NP. Figure 2(c) is the real-space optical microscopy image of the same area as that shown in Fig. 2(b), recorded while electrically exciting the NP located in the image center, using the STM. Here, the STM tip is located on the center of the cube's top face. Figure 2(d) shows in the inset an STM topography image of the same NP as in Fig. 2(b) ("NP1") and the STML spectra recorded with the tip located at two different points highlighted in the topography image, which we refer to as the "center" and "corner" in the following. For comparison purposes, the center and corner spectra are normalized so that they have the same intensity at the energy where the center spectrum exhibits its maximum. The difference between the two normalized spectra is plotted on the same graph. Similar measurements carried out on another NP in the same sample are shown in Fig. 2(e) ("NP2").

Upon STM excitation in the center of the NP, the emission spectrum exhibits a broad asymmetric profile, with a maximum at 1.81 eV and a shoulder in the near infrared (at about 1.35 eV). The real-space image recorded under the same conditions [see Fig. 2(c)] shows a perfectly symmetric doughnut-shaped spot with a pronounced intensity dip in the center, which is typical of an emitting dipole oriented along the optical axis (i.e., along z). This is confirmed by the cylindrical symmetry of the angular emission pattern observed in the corresponding Fourier-space image shown in Fig. 2(f). Thus the light measured under such conditions must result from the excitation of the out-of-plane dipolar resonance of the NP [13,57]. Based on these observations, we ascribe the peak at 1.81 eV to the out-of-plane dipolar plasmon mode of the NP. This assignment implies that the contribution of this mode to the STML spectra is redshifted by 0.36 eV in comparison to its expected resonance as measured using DFM.

The spectrum measured upon excitation on the corner of the NP is comparatively broader and its maximum is blueshifted to 1.87 eV. The corresponding Fourier-space image shown in Fig. 2(g) reveals the anisotropy of the angular emission pattern, where more light is emitted in the direction of the excited corner (i.e., $+\mathbf{k_x}$). Based on the simple model proposed in Refs. [13,57] (see Fig. S3 in the Supplemental Material [62]), we find that such a Fourier-space pattern may be considered generated by an effective emission dipole tilted by $25 \pm 5^\circ$ to the optical axis z. Nevertheless, the different dipolar contributions alone cannot explain the pronounced directivity of the emission toward $+\mathbf{k_x}$ at $|k_x/k_0| \geqslant 1$ in Fig. 2(g). The contribution of higher-order multipolar (e.g., quadrupolar) modes must be included [67]. Thus we infer that the difference between the center and corner spectra shown in Fig. 2(d), or in Fig. 2(e), results from the contribution of the in-plane dipolar mode and one or several higher-order multipolar modes of the NP. Due to the spectral width of these contributions, fitting these spectra with sets of Gaussian peaks may be very inaccurate, since a small change in the initial fitting parameters can lead to a large change in the result. Nevertheless, the comparison between the center and corner spectra made above reveals that the contribution of the in-plane dipolar mode to the STML spectra lies at a higher energy than that of the out-of-plane dipole. This is reversed compared to what is observed in DFM spectra and scattering cross section calculations. This switch in their order in energy results from the fact that the dipolar resonance along the z axis shifts more to the red as compared to the dipole along x, presumably due to the interaction with the tip. The possibility that such a switch occurs must be taken into account when analyzing STML spectra of plasmonic nanostructures in order to avoid the incorrect assignment of the STML peaks to plasmon modes known from other techniques (e.g., DFM).

B. Simulation results

1. Effect of near-field excitation and of the STM tip

We use numerical simulations to elucidate the origin of the discrepancies observed between the experimentally measured STML and DFM spectra. First, we neglect the possible effects that exist only when the experiments are carried out in air, i.e., we consider that the surrounding medium is vacuum in the simulations. In STML measurements, the presence of the tip and the fact that the excitation source is in the near field of the NP are expected to modify the optical response of the NP. This is in comparison to DFM measurements, where the NP responds to a plane wave propagating from the far field in the absence of a tip. In order to distinguish tip effects from the effect of near-field excitation in our calculations, we compare the far-field scattering spectrum of the NP (dotted and dashed lines) to the radiative response of the NP excited in its near field (solid lines), in the absence (red line) and in the presence of the tip (blue line) in Fig. 3.

The scattering cross sections shown in Fig. 3 are calculated for plane wave illuminations at normal and at grazing incidence (80°), in order to excite the in-plane and out-of-plane plasmon modes of the NP [see also Figs. S4(a) and S5 in the Supplemental Material [62]]. The far-field scattering of the NP is completely dominated by the resonances of its dipolar plasmon modes, the radiative contribution of its higher-order multipolar modes being negligible.

For the near-field excitation, we calculate the far-field emission of a z-oriented oscillating electric dipole ($\mathbf{p_z}$) located in the center and corner areas of the NP, in the absence of the tip. The dipolar and quadrupolar mode contributions can be identified on the basis of the charge-density distributions [see Figs. S4(b) and S6 in the Supplemental Material [62]]. Thus, in these numerical simulations of the STML experiment where the tip is omitted, we find that the emitted light in the far field is dominated by the dipolar mode of the NP along z. Nevertheless, non-negligible contributions from higher-order multipolar (e.g., quadrupolar) modes are also present.

The Fano-like profiles [30,68] of the radiation power spectra of $\mathbf{p_z}$ shown in Fig. 3 result from the far-field interference of the dipolar and quadrupolar modes. The extreme proximity of the excitation source to the NP favors the excitation of higher-order multipolar modes of the NP, which can coherently interfere with the dipolar modes in the far field if they

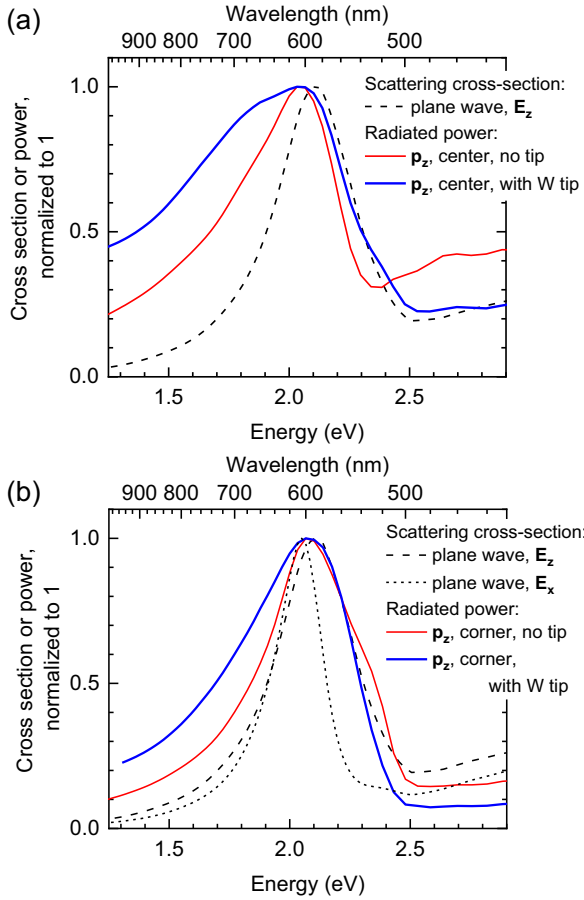

FIG. 3. Numerical simulations of the energy shifts and peak broadening due to tip and near-field excitation effects, which are present in experiments carried out in both air and vacuum. The surrounding medium (including the medium in the gap between the tip and the NP) has an index of refraction of 1. Dashed lines: scattering cross sections of a nanocube for *p*-polarized illumination [in (a) and (b)]. Dotted line: scattering cross section of a nanocube for *s*-polarized illumination [in (b)]. Solid lines: emission spectra for a **z**-oriented oscillating electric dipole located in the center [in (a)] and on the corner [in (b)] of the cube's top face in the absence (red line) and in the presence (blue line) of the tungsten (W) tip. All curves are normalized with respect to their maximum value.

spectrally overlap. In particular, on the high-energy side of the dipolar resonance, the two modes interfere destructively for $\mathbf{p_z}$ when the excitation is in the center and constructively for $\mathbf{p_z}$ when the excitation is at the corner. Globally, for $\mathbf{p_z}$ in the center, the interaction between the dipolar and quadrupolar modes broadens the radiation power spectrum on the low-energy side and narrows it on the high-energy side, thus leading to a redshift of the peak as compared to the scattering cross section of the NP. This effect, however, is not observed for $\mathbf{p_z}$ at the corner. Note that this effect is due to the fact that the lateral position of the local excitation source on the NP determines the phase relationship between the excited plasmon modes of the NP. These observations are in contrast to the case of far-field scattering, because plane waves propagating from the far field essentially excite the dipolar modes of the NP.

As shown in Fig. 3 (see blue lines), the addition of the tip in the calculations further broadens the emission peak, primarily

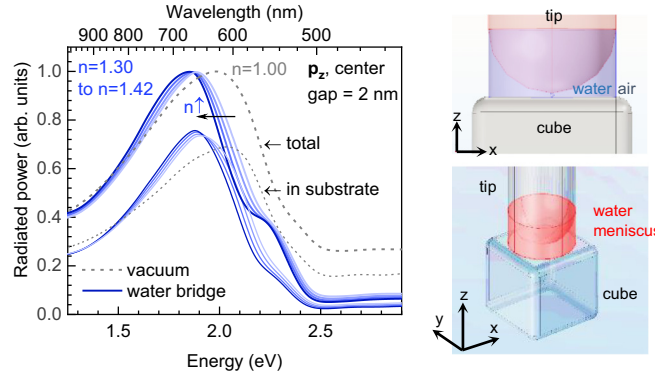

FIG. 4. Effect of the tip-sample water bridge. Similar calculations as in Fig. 3, but this time including the presence of a transparent medium of higher refractive index $n > 1$ (i.e., a water bridge) in the tip-sample gap. From right to left, the curves (blue lines) correspond to the results obtained for $n = 1.30$, 1.34, 1.38, and 1.42. A vertically (**z**)-oriented oscillating electric dipole located in the middle of a 2-nm-sized tip-sample gap, i.e., 1 nm above the center of the cube's top face, is considered. The right hand side of the figure shows the geometry of the water bridge considered in the calculations.

on its low-energy side. Similar observations are made for $\mathbf{p_z}$ on a corner, yet with smaller shift and peak broadening amplitudes (see also Figs. S7 to S9 in the Supplemental Material [62]). Additional simulations for various radii of curvature of the tip (ranging from 30 nm to 5 nm) have also been carried out, the results of which confirm our conclusions (see Fig. S10 in the Supplemental Material [62]).

In summary, our numerical simulations in vacuum show that the optical response of the NPs measured using STML is redshifted and broadened as compared to the scattering cross section of the same NP because of the NP-tip electromagnetic coupling and the contribution of higher-order multipolar modes of the NP, due to the near-field character of the inelastic-tunneling excitation. Evidently, such effects exist both in vacuum and in air. Figure 3 also confirms that the dipolar resonance of the NP along z shifts more to the red (more spectral broadening on the low-energy side of the peak) compared to the dipole along x, even when the effect of working in air is neglected.

2. Effect of the tip-sample water bridge

The numerical simulations presented in Fig. 3, where we consider that the dielectric medium in the tip-sample gap has an index of refraction of 1, are not enough to reproduce the complete shift of the emission peak to the red (to a value of 1.8 eV) as observed experimentally in Figs. 2(d) and 2(e). The presence of a water bridge in the tip-sample gap may explain the size of the experimentally observed redshift. Such a water bridge is expected to form when an STM is operated in air [39,40]. The increase of the local refractive index is expected to shift the plasmon resonances of the NP to lower energies due to charge screening effects. In order to verify this assumption, in Fig. 4, we carry out similar numerical calculations as in Fig. 3, but include a region between the tip and sample that has a higher refractive index ($n > 1$). This region has the shape of a cylinder of the same diameter as

the cylindrical part of the rod-shaped tip (30 nm) and fits the shape of the tip end (see the upper right panel of Fig. 4). In order to highlight the dependence of the spectral shift on n, we carry out the calculations for $n = 1.30$, 1.34, 1.38, and 1.42. Experimentally, refractive indexes higher than that of pure water ($n \approx 1.33$) may result from the presence of ligands around the NP, due to the synthesis method of colloidal NPs.

Figure 4 shows the results of these calculations where we consider that the tip is in the center of the cube's top face. A comparison with calculations carried out without including the water bridge (dotted lines in Fig. 4) reveals a clear narrowing of the emission peak on its higher-energy side, which yields a redshift of the peak center. Thick and thin lines in Fig. 4 correspond to the emission in full space (4π sr) or only in the substrate (lower half-space, 2π sr), where the STM-induced light is experimentally collected. Based on the similarity of the redshifts observed in the two cases, we rule out possible effects of emission anisotropy induced by the presence of the water bridge around the emitter. Therefore, we conclude that it is the local increase of the dielectric permittivity around the NP that induces the observed redshift of the simulated STML peak in Fig. 4, due to an additional screening effect. In agreement with this explanation, we observe that this redshift increases with the permittivity of the transparent medium in the tip-NP gap. Moreover, we have carried out simulations for various radii of the water bridge, ranging from 30 nm to 5 nm, while keeping the tip radius constant, and we found that (within this range) the radius of the water bridge has a negligible effect on the simulated STML spectra (see Fig. S11 in the Supplemental Material [62]). Indeed, the simulated STML spectra are most sensitive to the dielectric permittivity of the medium bridging the tip-sample gap within a few nanometer-wide region around the excitation source (i.e., the tunnel current in the experiment), where the electric field is concentrated.

Finally, the main experimental and theoretical results of this study are presented in Fig. 5. The spectra measured using the two different experimental techniques (i.e., DFM and STML) in order to probe the out-of-plane dipolar plasmon resonance of the NP are shown in Fig. 5(a). Their corresponding numerical simulations may be found in Fig. 5(b). A qualitative agreement between experiment and theory is obtained when the presence of the tip and of a water bridge in the tip-NP gap is taken into account, along with the near-field character of the excitation. In both experiment and theory, the STML spectral peak is shifted and broadened, as compared to what is obtained from light scattering. The near-field excitation, the effect of the tip, and the additional screening effect due to the water bridge in the STML experiments each contribute a significant part to the spectral shift and peak broadening. The remaining quantitative discrepancies between experiment and theory may result from simplifications of the STM tip geometry and the underestimation of the dielectric permittivity of the medium bridging the tip-sample gap, e.g., due to the residual presence of ligands in the adsorbed water.

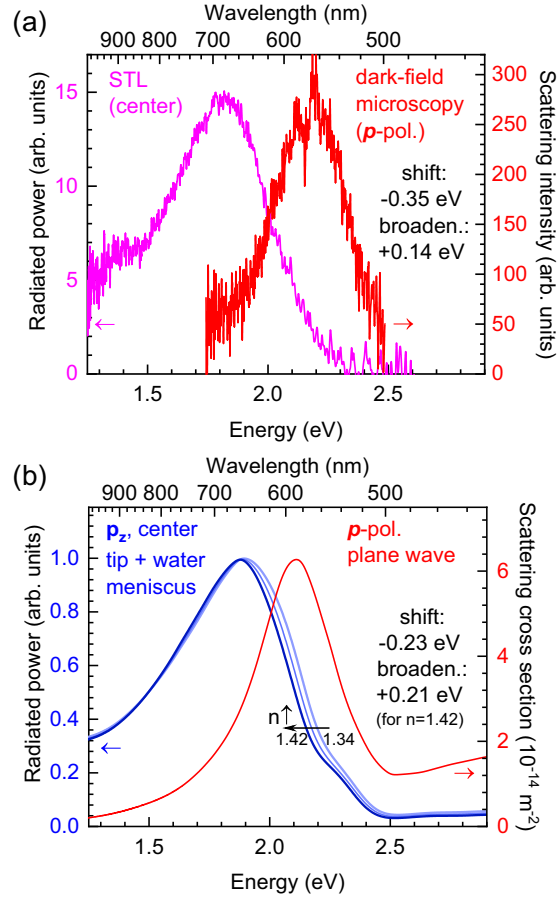

FIG. 5. Comparison: STML vs dark-field optical spectroscopy; experiment vs theory. (a) Light scattering spectrum of a single nanocube measured using dark-field optical spectroscopy under *p*-polarized illumination [same data as shown in Fig. 1(d)] and STML spectrum of a single nanocube upon local excitation with the tip located in the center of the cube's top face [same data as shown in Fig. 2(d)]. (b) Numerically calculated emission spectra for a vertically (**z**)-oriented oscillating electric dipole located 1 nm above the center of the cube's top face, in the absence and in the presence of the tungsten tip and water bridge [same data as shown in Figs. 1(d) and 4, respectively]. Experimentally, the STML peak shifts by −0.35 eV and is 0.14 eV wider than the DFM peak. Theoretically, the corresponding values are −0.23 eV and 0.21 eV.

IV. CONCLUSION

To conclude, we have used two methods for investigating the optical response of single plasmonic NPs, i.e., by measuring their light scattering spectra in a dark-field optical microscope (DFM) and their inelastic tunneling-induced luminescence under the tip of an STM (STML). Energy shifts, peak broadening, and a switch in the energy order of the dipolar resonances as compared to the expected (DFM-measured) resonances of the NP's modes are observed in STML, which hampers the identification of each emission band with an eigenmode of the NP. We have compared the experimental data obtained via STML and DFM to numerical simulations using the finite-element method. Numerical simulations of the STML experiments do not correctly reproduce the observed energy shifts if the effects of the surrounding atmosphere are not taken into account, i.e., if operations in vacuum are assumed in the model. We show that a better qualitative agreement between theory and experiment is obtained

if the presence of a water bridge in the gap between the STM tip and the NP is considered. Through this refinement of the numerical simulations, a more accurate interpretation of tip-induced electroluminescence spectra of single NPs is possible and errors in the assignment of the emission peaks to plasmon modes (known from light scattering measurements) of the NP may be avoided. Overall, our results will help in understanding the spectral shifts and peak broadening observed in virtually any optical measurement using a scanning probe microscope operated in air, where an emitter is located in the tip-sample gap or the tip-sample nanocavity itself emits light to the far field.

ACKNOWLEDGMENTS

We thank A. G. Borisov for helpful discussions along this project. This work is supported by a public grant overseen by the Agence Nationale de la Recherche (ANR) as part of the "Investissements d'Avenir" program (Labex NanoSaclay, Contract No. ANR-10-LABX-0035).

[1] P. Zijlstra and M. Orrit, Single metal nanoparticles: optical detection, spectroscopy and applications, Rep. Prog. Phys. **74**, 106401 (2011).

[2] C. Deeb, X. Zhou, R. Miller, S. K. Gray, S. Marguet, J. Plain, G. P. Wiederrecht, and R. Bachelot, Mapping the electromagnetic near-field enhancements of gold nanocubes, J. Phys. Chem. C **116**, 24734 (2012).

[3] J. Olson, S. Dominguez-Medina, A. Hoggard, L.-Y. Wang, W.-S. Chang, and S. Link, Optical characterization of single plasmonic nanoparticles, Chem. Soc. Rev. **44**, 40 (2015).

[4] F. Benz, C. Tserkezis, L. O. Herrmann, B. de Nijs, A. Sanders, D. O. Sigle, L. Pukenas, S. D. Evans, J. Aizpurua, and J. J. Baumberg, Nanooptics of molecular-shunted plasmonic nanojunctions, Nano Lett. **15**, 669 (2015).

[5] J. Nelayah, M. Kociak, O. Stéphan, F. J. García de Abajo, M. Tencé, L. Henrard, D. Taverna, I. Pastoriza-Santos, L. M. Liz-Marzán, and C. Colliex, Mapping surface plasmons on a single metallic nanoparticle, Nat. Phys. **3**, 348 (2007).

[6] F. J. García de Abajo, Optical excitations in electron microscopy, Rev. Mod. Phys. **82**, 209 (2010).

[7] P. Myrach, N. Nilius, and H.-J. Freund, Photon mapping of individual Ag particles on MgO/Mo(001), Phys. Rev. B **83**, 035416 (2011).

[8] L. Douillard and F. Charra, High-resolution mapping of plasmonic modes: Photoemission and scanning tunnelling luminescence microscopies, J. Phys. D: Appl. Phys. **44**, 464002 (2011).

[9] V. Myroshnychenko, J. Nelayah, G. Adamo, N. Geuquet, J. Rodríguez-Fernández, I. Pastoriza-Santos, K. F. MacDonald, L. Henrard, L. M. Liz-Marzán, N. I. Zheludev, M. Kociak, and F. J. García de Abajo, Plasmon spectroscopy and imaging of individual gold nanodecahedra: A combined optical microscopy, cathodoluminescence, and electron energy-loss spectroscopy study, Nano Lett. **12**, 4172 (2012).

[10] V. Iberi, N. Mirsaleh-Kohan, and J. P. Camden, Understanding plasmonic properties in metallic nanostructures by correlating photonic and electronic excitations, J. Phys. Chem. Lett. **4**, 1070 (2013).

[11] A. Hörl, A. Trügler, and U. Hohenester, Full three-dimensonal reconstruction of the dyadic Green tensor from electron energy loss spectroscopy of plasmonic nanoparticles, ACS Photon. **2**, 1429 (2015).

[12] A. C. Atre, B. J. M. Brenny, T. Coenen, A. García-Etxarri, A. Polman, and J. A. Dionne, Nanoscale optical tomography with cathodoluminescence spectroscopy, Nat. Nanotechnol. **10**, 429 (2015).

[13] E. Le Moal, S. Marguet, D. Canneson, B. Rogez, E. Boer-Duchemin, G. Dujardin, T. V. Teperik, D.-C. Marinica, and A. G. Borisov, Engineering the emission of light from a scanning tunneling microscope using the plasmonic modes of a nanoparticle, Phys. Rev. B **93**, 035418 (2016).

[14] A. Yu, S. Li, G. Czap, and W. Ho, Tunneling-electron-induced light emission from single gold nanoclusters, Nano Lett. **16**, 5433 (2016).

[15] S. Mitiche, S. Marguet, F. Charra, and L. Douillard, Near-field localization of single Au cubes: A group theory description, J. Phys. Chem. C **121**, 4517 (2017).

[16] S. Cao, M. Zapata-Herrera, A. Campos, E. Le Moal, S. Marguet, G. Dujardin, M. Kociak, J. Aizpurua, A. G. Borisov, and E. Boer-Duchemin, Probing the radiative electromagnetic local density of states in nanostructures with a scanning tunneling microscope, ACS Photon. **7**, 1280 (2020).

[17] J. Lambe and S. L. McCarthy, Light emission from inelastic electron tunneling, Phys. Rev. Lett. **37**, 923 (1976).

[18] D. Hone, B. Mühlschlegel, and D. J. Scalapino, Theory of light emission from small particle tunnel junctions, Appl. Phys. Lett. **33**, 203 (1978).

[19] R. W. Rendell, D. J. Scalapino, and B. Mühlschlegel, Role of local plasmon modes in light emission from small-particle tunnel junctions, Phys. Rev. Lett. **41**, 1746 (1978).

[20] J. K. Gimzewski, J. K. Sass, R. R. Schlitter, and J. Schott, Enhanced photon emission in scanning tunnelling microscopy, Europhys. Lett. **8**, 435 (1989).

[21] P. Johansson, R. Monreal, and P. Apell, Theory for light emission from a scanning tunneling microscope, Phys. Rev. B **42**, 9210 (1990).

[22] R. Berndt, J. K. Gimzewski, and P. Johansson, Inelastic tunneling excitation of tip-induced plasmon modes on noble-metal surfaces, Phys. Rev. Lett. **67**, 3796 (1991).

[23] M. G. Boyle, J. Mitra, and P. Dawson, Infrared emission from tunneling electrons: The end of the rainbow in scanning tunneling microscopy, Appl. Phys. Lett. **94**, 233118 (2009).

[24] M. Parzefall and L. Novotny, Light at the end of the tunnel, ACS Photon. **5**, 4195 (2018).

[25] A. Martín-Jiménez, A. I. Fernández-Domínguez, K. Lauwaet, D. Granados, R. Miranda, F. J. García-Vidal, and R. Otero, Unveiling the radiative local density of optical states of a plasmonic nanocavity by STM, Nat. Commun. **11**, 1021 (2020).

[26] F. Silly, A. O. Gusev, A. Taleb, F. Charra, and M.-P. Pileni, Coupled plasmon modes in an ordered hexagonal monolayer of metal nanoparticles: A direct observation, Phys. Rev. Lett. **84**, 5840 (2000).

[27] N. Nilius, N. Ernst, and H.-J. Freund, Photon emission spectroscopy of individual oxide-supported silver clusters in a scanning tunneling microscope, Phys. Rev. Lett. **84**, 3994 (2000).

[28] N. Nilius, N. Ernst, and H.-J. Freund, Photon emission from individual supported gold clusters: thin film versus bulk oxide, Surf. Sci. **478**, L327 (2001).

[29] D. V. Lebedev, V. A. Shkoldin, A. M. Mozharov, D. V. Permyakov, L. N. Dvoretckaia, A. A. Bogdanov, A. K. Samusev, A. O. Golubok, and I. S. Mukhin, Scanning tunneling microscopy-induced light emission and I(V) study of optical near-field properties of single plasmonic nanoantennas, J. Phys. Chem. Lett. **12**, 501 (2021).

[30] Y. Ma, O. J. F. Martin, and A. Stemmer, Selectively exciting and probing radiative plasmon modes on short gold nanorods by scanning tunneling microscope-induced light emission, ACS Photon. **10**, 743 (2023).

[31] N. Nilius, N. Ernst, and H.-J. Freund, Tip influence on plasmon excitations in single gold particles in an STM, Phys. Rev. B **65**, 115421 (2002).

[32] A. García-Etxarri, I. Romero, F. J. García de Abajo, R. Hillenbrand, and J. Aizpurua, Influence of the tip in near-field imaging of nanoparticle plasmonic modes: Weak and strong coupling regimes, Phys. Rev. B **79**, 125439 (2009).

[33] T. Wang, E. Boer-Duchemin, Y. Zhang, G. Comtet, and G. Dujardin, Excitation of propagating surface plasmons with a scanning tunnelling microscope, Nanotechnology **22**, 175201 (2011).

[34] P. Bharadwaj, A. Bouhelier, and L. Novotny, Electrical excitation of surface plasmons, Phys. Rev. Lett. **106**, 226802 (2011).

[35] T. Wang, B. Rogez, G. Comtet, E. Le Moal, W. Abidi, H. Remita, G. Dujardin, and E. Boer-Duchemin, Scattering of electrically excited surface plasmon polaritons by gold nanoparticles studied by optical interferometry with a scanning tunneling microscope, Phys. Rev. B **92**, 045438 (2015).

[36] B. Rogez, R. Horeis, E. Le Moal, J. Christoffers, K. Al-Shamery, G. Dujardin, and E. Boer-Duchemin, Optical and electrical excitation of hybrid guided modes in an organic nanofiber-gold film system, J. Phys. Chem. C **119**, 22217 (2015).

[37] S. Cao, E. Le Moal, F. Bigourdan, J.-P. Hugonin, J.-J. Greffet, A. Drezet, S. Huant, G. Dujardin, and E. Boer-Duchemin, Revealing the spectral response of a plasmonic lens using low-energy electrons, Phys. Rev. B **96**, 115419 (2017).

[38] J. A. Dagata, J. Schneir, H. H. Harary, C. J. Evans, M. T. Postek, and J. Bennett, Modification of hydrogen-passivated silicon by a scanning tunneling microscope operating in air, Appl. Phys. Lett. **56**, 2001 (1990).

[39] M. G. Boyle, J. Mitra, and P. Dawson, The tip-sample water bridge and light emission from scanning tunnelling microscopy, Nanotechnology **20**, 335202 (2009).

[40] B. Rogez, S. Cao, G. Dujardin, G. Comtet, E. Le Moal, A. Mayne, and E. Boer-Duchemin, The mechanism of light emission from a scanning tunnelling microscope operating in air, Nanotechnology **27**, 465201 (2016).

[41] V. A. Shkoldin, D. V. Permyakov, K. S. Ladutenko, M. V. Zhukov, A. A. Vasiliev, A. O. Golubok, A. V. Uskov, A. D. Bolshakov, A. A. Bogdanov, A. K. Samusev, and I. S. Mukhin, Crucial role of metal surface morphology in photon emission from a tunnel junction at ambient conditions, J. Phys. Chem. C **123**, 8813 (2019).

[42] T. V. Teperik, A. K. Kazansky, and A. G. Borisov, Electron tunneling through water layer in nanogaps probed by plasmon resonances, Phys. Rev. B **93**, 155431 (2016).

[43] S. Gómez-Moñivas, J. J. Sáenz, M. Calleja, and R. García, Field-induced formation of nanometer-sized water bridges, Phys. Rev. Lett. **91**, 056101 (2003).

[44] G. M. Sacha, A. Verdaguer, and M. Salmeron, Induced water condensation and bridge formation by electric fields in atomic force microscopy, J. Phys. Chem. B **110**, 14870 (2006).

[45] T. Cramer, F. Zerbetto, and R. García, Molecular mechanism of water bridge buildup: Field-induced formation of nanoscale menisci, Langmuir **24**, 6116 (2008).

[46] Y. Men, X. Zhang, and W. Wang, Capillary liquid bridges in atomic force microscopy: Formation, rupture, and hysteresis, J. Chem. Phys. **131**, 184702 (2009).

[47] T. Thundat, X.-Y. Zheng, G. Chen, and R. Warmack, Role of relative humidity in atomic force microscopy imaging, Surf. Sci. Lett. **294**, L939 (1993).

[48] M. Luna, J. Colchero, and A. Baró, Intermittent contact scanning force microscopy: The role of the liquid necks, Appl. Phys. Lett. **72**, 3461 (1998).

[49] H. Bloeß, G. Staikov, and J. Schultze, AFM induced formation of SiO_2 structures in the electrochemical nanocell, Electrochim. Acta **47**, 335 (2001).

[50] Z. Wei and Y.-P. Zhao, Growth of liquid bridge in AFM, J. Phys. D: Appl. Phys. **40**, 4368 (2007).

[51] S. H. Yang, M. Nosonovsky, H. Zhang, and K.-H. Chung, Nanoscale water capillary bridges under deeply negative pressure, Chem. Phys. Lett. **451**, 88 (2008).

[52] J. Toset and G. Gomila, Three-dimensional manipulation of gold nanoparticles with electro-enhanced capillary forces, Appl. Phys. Lett. **96**, 043117 (2010).

[53] J.-W. Liou and W.-Y. Woon, Revisiting oxidation scanning probe lithography of graphene: Balance of water condensation energy and electrostatic energy, J. Phys. Chem. C **123**, 25422 (2019).

[54] S. Davy, M. Spajer, and D. Courjon, Influence of the water layer on the shear force damping in near-field microscopy, Appl. Phys. Lett. **73**, 2594 (1998).

[55] P. K. Wei and W. S. Fann, The effect of humidity on probe-sample interactions in near-field scanning optical microscopy, J. Appl. Phys. **87**, 2561 (2000).

[56] F. M. Huang, F. Culfaz, F. Festy, and D. Richards, Effect of the surface water layer on the optical signal in apertureless scanning near field optical microscopy, Nanotechnology **18**, 015501 (2007).

[57] E. Le Moal, S. Marguet, B. Rogez, S. Mukherjee, P. Dos Santos, E. Boer-Duchemin, G. Comtet, and G. Dujardin, An electrically excited nanoscale light source with active angular control of the emitted light, Nano Lett. **13**, 4198 (2013).

[58] R. Esteban, A. G. Borisov, P. Nordlander, and J. Aizpurua, Bridging quantum and classical plasmonics with a quantum-corrected model, Nat. Commun. **3**, 825 (2012).

[59] J. J. Baumberg, J. Aizpurua, M. H. Mikkelsen, and D. R. Smith, Extreme nanophotonics from ultrathin metallic gaps, Nat. Mater. **18**, 668 (2019).

[60] M. Haggui, M. Dridi, J. Plain, S. Marguet, H. Perez, G. C. Schatz, G. P. Wiederrecht, S. K. Gray, and R. Bachelot,

Spatial confinement of electromagnetic hot and cold spots in gold nanocubes, ACS Nano **6**, 1299 (2012).

[61] J. Deumer, B. R. Pauw, S. Marguet, D. Skroblin, O. Taché, M. Krumrey, and C. Gollwitzer, Small-angle X-ray scattering: characterization of cubic Au nanoparticles using Debye's scattering formula, J. Appl. Crystallogr. **55**, 993 (2022).

[62] See Supplemental Material at http://link.aps.org/supplemental/10.1103/PhysRevB.109.155433 for scanning electron micrographs of plasmonic nanoparticles, optical extinction spectrum measured in solution, analysis of Fourier-space images, and supplementary numerical simulations, which also includes Ref. [69].

[63] Y. Zhang, E. Boer-Duchemin, T. Wang, B. Rogez, G. Comtet, E. Le Moal, G. Dujardin, A. Hohenau, C. Gruber, and J. R. Krenn, Edge scattering of surface plasmons excited by scanning tunneling microscopy, Opt. Express **21**, 13938 (2013).

[64] S. Cao, E. Le Moal, E. Boer-Duchemin, G. Dujardin, A. Drezet, and S. Huant, Cylindrical vector beams of light from an electrically excited plasmonic lens, Appl. Phys. Lett. **105**, 111103 (2014).

[65] B. N. J. Persson and A. Baratoff, Theory of photon emission in electron tunneling to metallic particles, Phys. Rev. Lett. **68**, 3224 (1992).

[66] P. Johansson, Light emission from a scanning tunneling microscope: Fully retarded calculation, Phys. Rev. B **58**, 10823 (1998).

[67] T. Coenen, F. B. Arango, A. F. Koenderink, and A. Polman, Directional emission from a single plasmonic scatterer, Nat. Commun. **5**, 3250 (2014).

[68] S. Zhang, K. Bao, N. J. Halas, H. Xu, and P. Nordlander, Substrate-induced Fano resonances of a plasmonic nanocube: A route to increased-sensitivity localized surface plasmon resonance sensors revealed, Nano Lett. **11**, 1657 (2011).

[69] K. Joulain, R. Carminati, J.-P. Mulet, and J.-J. Greffet, Definition and measurement of the local density of electromagnetic states close to an interface, Phys. Rev. B **68**, 245405 (2003).